

# NON-ITERATIVE NUMERICAL IMPLEMENTATION FOR THE CONSTITUTIVE MODELLING OF PRESSURE-DEPENDENT ELASTOPLASTICITY USING PARABOLOIDAL YIELD CRITERIA

V. LAHERI<sup>a,\*</sup>, P. HAO<sup>a,b</sup> AND F. A. GILABERT<sup>a</sup>

<sup>a</sup> Ghent University, Department of Materials, Textiles and Chemical Engineering  
Technologiepark-Zwijnaarde 46, 9052 Zwijnaarde, Belgium.

\* Corresponding author: vikram.laheri@ugent.be  
web page: <https://materialmodels.ugent.be/>

<sup>b</sup> SIM Program, M3Strength  
Technologiepark-Zwijnaarde 48, 9052 Zwijnaarde, Belgium.

**Key words:** Continuum mechanics, computational methods, flow rule, paraboloidal yield criterion, pressure-dependent elastoplasticity, polymer matrix.

**Abstract.** A full understanding of the non-linear mechanical response of the polymer is essential for fibre-reinforced polymer composite design because an explicit definition of constitutive material models for the constituents (fibres, matrix, and interface) are prerequisite in micromechanical simulation. Unlike metals, the material behaviour of the polymer matrix is modelled by plasticity theories using a combination of distortional and spherical energy dissipation. In this respect, an elastoplastic thermodynamic continuum model derivation is proposed using the paraboloidal yield criterion under isothermal conditions. A non-iterative scheme is developed for the numerical computation of the plastic strain increment multiplier. Both associated and non-associated flow rules are investigated following classical plasticity loading-unloading conditions. It thereby, evades the conventional computationally demanding iterative process by replacing it with an exact determination of plastic strain increment. This novel approach highly improves the computational efficiency algorithmically. Coupon-sized numerical models are investigated and the comparison between simulated and experimental results shows the reliability and unprecedented accuracy of the proposed elastoplastic mathematical model.

## 1 INTRODUCTION

The approach to improve the mechanical performance of fibre-reinforced polymer composites at lower scales relies on micromechanical modelling of the representative volume elements combined with homogenisation techniques so that a detailed expression of the mechanical response can be provided. Besides the fibres, the mechanical response of the polymer matrix plays a crucial role in the overall composite performance. Due to the highly non-linear nature of polymers, a robust and consistent numerical treatment of its material model is needed.

The pressure-dependent plastic behaviour is an inherent feature in polymer matrices. The paraboloidal yield criterion propounded by Tschoegl [1] is adopted to describe pressure-dependent plasticity, which represents a paraboloid surface in the triaxial principal stress coordinates system. It meets the requirement for a closed surface avoiding angular apex in pure tensile and an open surface in pure compressive octants. The elastoplastic computational implementation developed by Melro *et al.* [2] computes plastic strain increment using a computationally demanding iterative approximation technique based on Newton-Raphson's method that does not always succeed under very large deformations.

This research aims at developing an efficient and exact implementation of the elastoplastic constitutive model with the paraboloidal plasticity theory. With this novel implementation, the evolution of plastic strain is computed by using a non-iterative scheme with high accuracy. This is achieved by solving the quadratic equation of the yield criterion described as a function of plastic strain increment, obtained using the update of trial stress from radial return mapping algorithm. This procedure diminishes the computational time and avoids the risk of aggregating approximation errors that lead to convergence solver issues. For verification, the proposed implementation is numerically investigated in two levels of benchmark examples: (i) simple single-element test to observe its functionality, (ii) cylinder compression test to analyse convergence and mesh sensitivity.

## 2 CONTINUUM MECHANICS

To determine the elastoplastic constitutive relationship of the polymer material the Clausius-Dunham's entropy inequality for isothermal process is employed given by

$$\boldsymbol{\sigma} : \dot{\boldsymbol{\varepsilon}} - \dot{\Psi} \geq 0, \quad (2.1)$$

where  $\boldsymbol{\sigma}$  and  $\boldsymbol{\varepsilon}$  are the stress and strain tensors, respectively and  $\Psi$  is the Helmholtz energy function considering isotropic hardening.

### 2.1 Yield Criterion

The paraboloidal yield criterion as a function of stress tensor and yield stresses in tension ( $\sigma_t$ ), and compression ( $\sigma_c$ ) is given by

$$\phi(\boldsymbol{\sigma}) = \bar{\sigma}^2 - (\sigma_t - \sigma_c) I_1 - \sigma_t \sigma_c, \quad (2.2)$$

where  $\bar{\sigma} = \sqrt{\frac{3}{2} \boldsymbol{\sigma}' : \boldsymbol{\sigma}'}$  is the equivalent (von Mises) stress and the pressure-dependent term,  $I_1 = \boldsymbol{\sigma} : \mathbf{I} = -3p$  is the first invariant of stress tensor.

### 2.2 Constitutive modelling

Owing to the associative split of strain ( $\boldsymbol{\varepsilon} = \boldsymbol{\varepsilon}^e + \boldsymbol{\varepsilon}^p$ ) and applying the Coleman-Noll statement for thermodynamic equilibrium of the process variable  $\boldsymbol{\varepsilon}^e$  [3] on the inequality eq. (2.1), the 2<sup>nd</sup> order linear elastic initiation is given by

$$\boldsymbol{\sigma} = \frac{\partial \Psi^e}{\partial \boldsymbol{\varepsilon}^e} = 2\mu \boldsymbol{\varepsilon}^{e'} + \kappa(\boldsymbol{\varepsilon}^e : \mathbf{I}) \mathbf{I}. \quad (2.3)$$

The superscripts, “ $e$ ” and “ $p$ ” denotes the elastic and plastic parts, respectively. The elastic tangent modulus,  $\mathbb{C}^e$  is a 4<sup>th</sup> order tensor is thus, defined as

$$\mathbb{C}^e = \frac{\partial^2 \Psi^e}{\partial \boldsymbol{\varepsilon}^e \partial \boldsymbol{\varepsilon}^e} = 2\mu \mathbb{P} + \kappa \bar{\mathbb{I}}, \quad (2.4)$$

where  $\bar{\mathbb{I}}$  is the hydrostatic operator, and  $\mathbb{P}$  is the projection tensor.

Reformulation of the reduced internal dissipation of inequality as an optimisation problem yields the Kuhn-Tucker’s loading-unloading consistency conditions that demands

$$\Delta\gamma \geq 0; \quad \phi \leq 0; \quad \Delta\gamma \phi = 0. \quad (2.5)$$

The plastic strain increment,  $\Delta\gamma$  and flow direction tensor,  $\boldsymbol{\eta}$  at yield are governed by the gradient of the plastic flow potential.

### 2.3 Associated flow rule

Associated flow rule implies that the plastic flow develops along the normal to the predicted yield surface, denoted by “ $tr$ ” and expressed as

$$\boldsymbol{\eta} = \frac{\partial \phi^{tr}}{\partial \boldsymbol{\sigma}^{tr}} = 3\boldsymbol{\sigma}^{tr'} - (\sigma_t - \sigma_c) \mathbf{I}. \quad (2.6)$$

Using radial return mapping algorithm to determine  $\Delta\gamma$ , we get

$$\boldsymbol{\sigma}_{n+1} = \boldsymbol{\sigma}_{n+1}^{tr} - \Delta\gamma \left[ 6\mu \boldsymbol{\sigma}^{tr'} - 3\kappa (\sigma_t - \sigma_c) \mathbf{I} \right]. \quad (2.7)$$

Upon rearranging the relations of stress invariants, the yielding can be represented as a function of  $\Delta\gamma$ . Its quadratic solution yields the values of  $\Delta\gamma$  as follows

$$\phi(\Delta\gamma) = \phi^{tr} + 4\bar{\sigma}^{tr2} (9\mu^2 - h^2) \Delta\gamma^2 - \left[ 12\mu\bar{\sigma}^{tr2} + 2h(\sigma_t + \sigma_c)\bar{\sigma}^{tr} + 9\kappa(\sigma_t - \sigma_c)^2 \right] \Delta\gamma \quad (2.8)$$

The consistent elastoplastic tangent modulus is the tensorial differentiation of updated stress (refer equation 2.7) derived as

$$\mathbb{C}^{ep} = \frac{\partial \boldsymbol{\sigma}}{\partial \boldsymbol{\varepsilon}^e} = \mathbb{C}^e - \{ \mathbb{C}^e : \boldsymbol{\eta} \} \otimes \frac{\partial \Delta\gamma}{\partial \boldsymbol{\varepsilon}^{e,tr}} - \Delta\gamma \frac{\partial \{ \mathbb{C}^e : \boldsymbol{\eta} \}}{\partial \boldsymbol{\varepsilon}^{e,tr}}. \quad (2.9)$$

### 2.4 Non-associated flow rule

Following the deductions of Kolling *et al.* [4] the flow potential function is given by

$$g = \bar{\sigma}^2 + \frac{\alpha_0}{9} I_1^2, \quad (2.10)$$

where  $\alpha_0$  is the coefficient associating to the volumetric part of plastic flow dependent upon the plastic Poisson’s ratio,  $\nu^p$ . Duncan *et al.* [5] showed that as an indicator to volume increase during plastic yielding,  $\nu^p$  ranges between 0.3 and 0.5. The pressure-dependent coefficient  $\alpha_0$  as a function of  $\nu^p$  is defined as

$$\alpha_0(\nu^p) = \frac{9}{2} \left( \frac{1 - 2\nu^p}{1 + \nu^p} \right). \quad (2.11)$$

The flow normal is tangential to the predicted flow potential,  $g^{tr}$  redefined as

$$\boldsymbol{\eta} = \frac{\partial g^{tr}}{\partial \boldsymbol{\sigma}^{tr}} = 3\boldsymbol{\sigma}^{tr'} + \frac{2}{9}\alpha_0 I_1^{tr} \mathbf{I}. \quad (2.12)$$

Using the stress update using radial return mapping algorithm, we get

$$\boldsymbol{\sigma}_{n+1} = \boldsymbol{\sigma}_{n+1}^{tr} - \Delta\gamma \left( 6\mu \boldsymbol{\sigma}^{tr'} + \frac{2}{3}\kappa \alpha_0 I_1 \mathbf{I} \right). \quad (2.13)$$

The yield surface function is also redefined for the quadratic solutions of  $\Delta\gamma$  as

$$\phi(\Delta\gamma) = \phi^{tr} + 4\bar{\sigma}^{tr2} (9\mu^2 - h^2) \Delta\gamma^2 - \left[ 12\mu\bar{\sigma}^{tr2} + 2h(\sigma_t + \sigma_c)\bar{\sigma}^{tr} - 2\kappa\alpha_0(\sigma_t - \sigma_c)I_1^{tr} \right] \Delta\gamma. \quad (2.14)$$

The consistent elastoplastic tangent modulus is expressed similarly as in (2.9). The partial differentiations of the terms in elastoplastic tangent operator however, differs.

### 3 NUMERICAL IMPLEMENTATION

The elastic predictor approach ensuing radial return algorithm is an empirically heuristic method for numerical modelling of elastoplasticity. Implementation of the finite element computation is manoeuvred to determine and eliminate the plastic part from the total strain, resulting in the overall elastic effect.

---

**Algorithm 1:**  $\Delta\gamma$  computation using proposed model.

---

```

1 ▷ Get  $\Delta\gamma_n \leftarrow$  state variable
2 ▷ Initialise:  $\Delta\gamma_{n+1} \leftarrow \Delta\gamma_n$  // back-up value
3 ▷ Discriminant:  $\Delta = b^2 - 4ac$ 
   ► Determine if  $\Delta$  is positive, for real roots:
4 if ( $\Delta \geq 0$ ) then
5     ▷ Compute roots:  $\Delta\gamma_{1,2} = \frac{-b \pm \sqrt{\Delta}}{2a}$ 
6     ▷ Compute function values:  $\phi_{1,2} = a \Delta\gamma_{1,2}^2 + b \Delta\gamma_{1,2} + \phi^{tr}$ 
   ► Determine the root following Kuhn-Tucker's loading-unloading conditions:
7     if ( $\Delta\gamma_1 \geq 0$  and  $\phi_1 \leq 0$  and  $\Delta\gamma_1 \cdot \phi_1 = 0$ ) then
8       Result:  $\Delta\gamma_{n+1} \leftarrow \Delta\gamma_1$ 
9     else if ( $\Delta\gamma_2 \geq 0$  and  $\phi_2 \leq 0$  and  $\Delta\gamma_2 \cdot \phi_2 = 0$ ) then
10      Result:  $\Delta\gamma_{n+1} \leftarrow \Delta\gamma_2$ 
9 return:  $\Delta\gamma_{n+1}$ 

```

---

A school of thought [7, 6, 8, 9, 10, 11, 12, 13, 14, 15] following the works of Melro *et al.* [2], employs Newton-Raphson's iterative numerical approach to solve the non-linear system of equations to determine an approximate value of  $\Delta\gamma$ . The convergence rate of the iterative approximation approach is quadratic and inexact, causing accumulation of

error for stress and tangent modulus computation. The order of magnitude of the initial guess,  $\Delta\gamma^0$  and iterative computation of the associated residual function,  $\partial\phi/\partial\Delta\gamma$  forms a decisive factor for the rate of convergent solution determination. If the results are divergent in an arbitrarily limited number of iterations,  $n_{iter}$ , the computation process demands improving  $\Delta\gamma^{(0)}$  algorithmically and repeating the iterative scheme. The iterative steps geometrically progress to  $n_{iter} \times n_{fail}$ , where  $n_{fail}$  are the number of failed attempts.

With the mathematical model proposed in this work, the algorithm 1 follows a direct computation as the root of a quadratic equations (2.8) and (2.14).

The proposed algorithm qualifies to eliminate the iterative scheme thereby making it computationally frugal. The proposed model is also computationally robust as the solution of non-linear equation of  $\Delta\gamma$  is absolute and algorithmically efficient with no iterative looping. The approach straightforwardly processes on the classical loading-unloading conditions (2.5) to accurately determine a unique  $\Delta\gamma$ .

## 4 NUMERICAL INVESTIGATIONS

For numerical validation, the proposed non-iterative scheme of the constitutive elastoplastic models (refer section 2) is implemented as a user material subroutine **UMAT** in a commercial finite element software. For elastoplastic response of epoxy polymer, the reference material parameters of a typical thermosetting plastic are used.

### 4.1 Data preparation

Guild *et al.* [16] predicted a constant value of  $\nu^p = 0.32$  as the best fit for epoxy. Table 1 encapsulates the elastoplastic material properties for a typical epoxy resin used in the numerical simulation. Adapted from [17] are the experimentally determined elastic moduli,  $E_t$  and  $E_c$  and the yield stresses,  $\sigma_t$  and  $\sigma_c$  at the onset of plasticity in tension and compression, respectively.

**Table 1:** Material properties for epoxy resin.

	Material parameters	Values	Units
Elastic	$E$	3760	MPa
	$\nu$	0.39	~
	$\nu^p$	0.32	~
Plastic	$\sigma_t$	29	MPa
	$\sigma_c$	67	MPa
Experimentally determined	$E_t$	3900	MPa
	$E_c$	3600	MPa

The plastic strains corresponding to yield stresses are extracted by

$$\epsilon_{\{\lambda\}}^p = \epsilon - \frac{\sigma}{E_{\{\lambda\}}} \quad \forall\{\lambda\} = \begin{cases} t : \text{tension} \\ c : \text{compression} \end{cases} \quad (4.1)$$

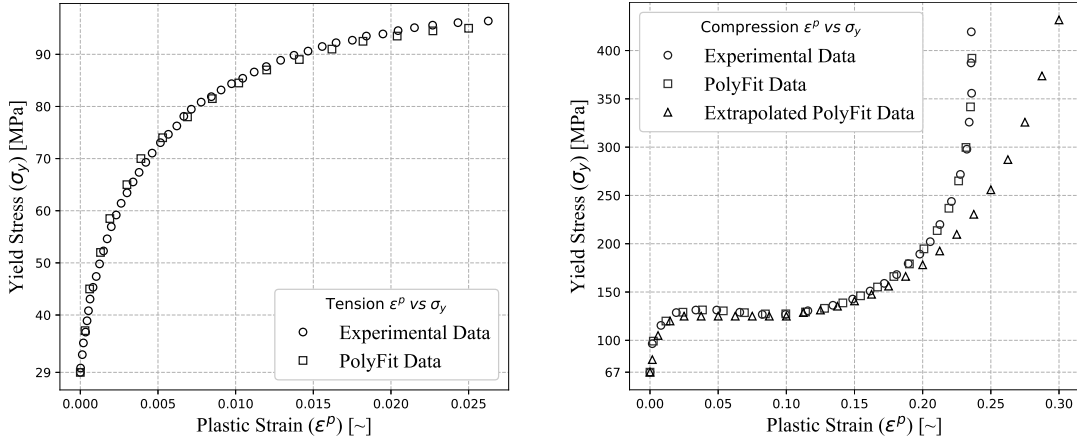


**Figure 1:** Evolution of  $\sigma_y$  with respect to  $\epsilon^p$ .

where  $\sigma$  is the stress after yielding for the corresponding strain,  $\epsilon$ . An equally spaced data of plastic strain corresponding to yield stress for hardening computation is generated as shown in the figure 1.

The data in the very large rubber-like deformation domain in compression is assumed and extrapolated to pseudo-plastic response by adding instantaneous stiffness,  $E_{inst}$  values to Young's modulus so that the plasticity model with isotropic hardening can be employed.

$$\epsilon_c^p = \epsilon - \frac{\sigma}{E_c + E_{inst}}. \quad (4.2)$$

## 4.2 Single element test

A three-dimensional single element model of 1 mm length is depicted in figure 2 with corresponding boundary conditions tabulated. It is used to numerically verify with the experimental results obtained by Feidler *et al.* [17] under tensile, compressive, and shear loading conditions employing both the flow rules. This simple geometry helps to verify the functioning of the material model reliably.

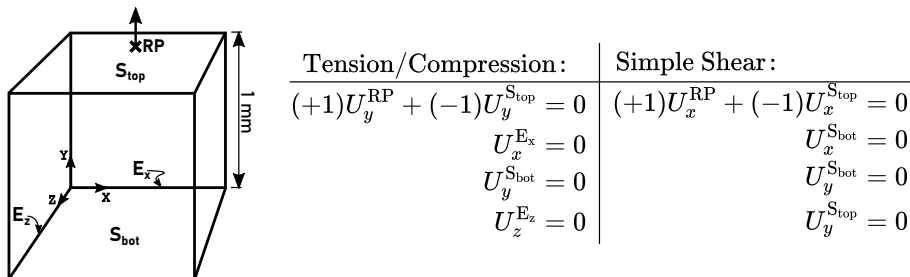


**Figure 2:** Boundary conditions and the single element test.

The graphs in figure 3 for both the flow rules conform to the elastoplastic experimental curves subjected to the three loading modes under small strain conditions. In compression mode at large strain under the provision of pseudo-plastic hardening, the numerical result

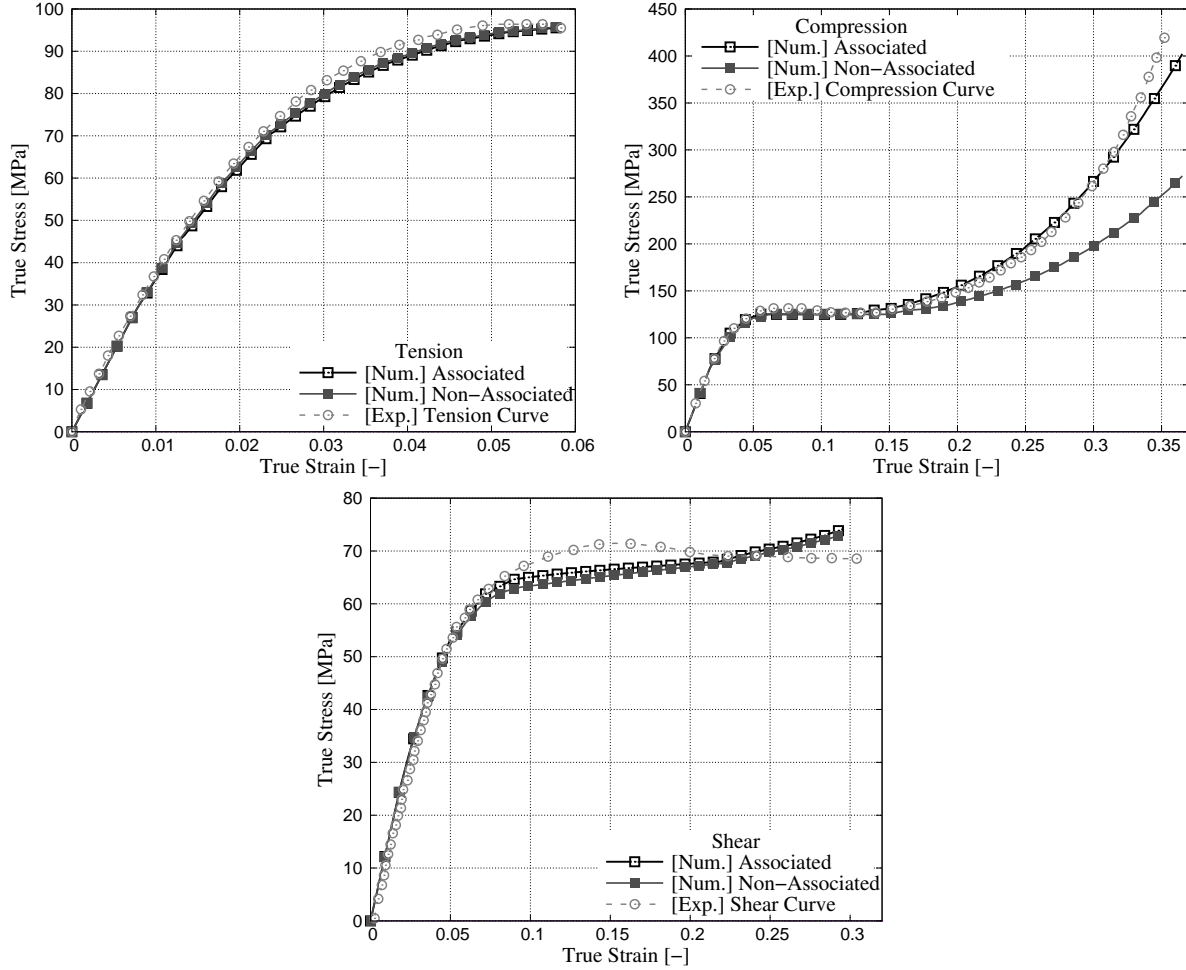


**Figure 3:** Stress-strain relationship from the single element test.

for the associated flow rule shows a higher degree of conformance with the experiment compared to the associated flow rule. This deviation can be attributed to the hydrostatic sensitivity owing to the presence of the pressure correction term applied in the non-associated flow potential function,  $g$  (2.10). Numerical modelling in shear also uses the constitutive relationship, predominantly relying on the tensile and compressive yield stress regardless of the yielding properties in shear. Therefore, the numerical results in graph show less agreement with the experiment at large strain.

### 4.3 Cylinder compression test

To simulate a cylinder specimen under compression, a one-eighth ( $1/8$ ) symmetrical model and corresponding boundary conditions are used, as shown in the figure 4. The model is tested with different element sizes using the proposed non-iterative mathematical simulation. The dimensions shown on a meshed instance with element size,  $\ell_{elem} = 1$  mm are  $H = 6$  mm and  $R = 6$  mm. The compression of the cylinder is assumed frictionless.

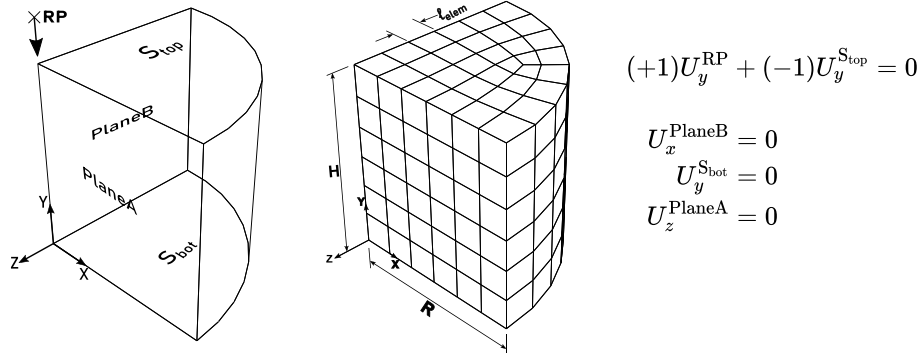


**Figure 4:** Cylinder compression test specimen and boundary conditions. (Left): Symmetrical model set-up. (Right): Finite element mesh and geometrical dimensions.

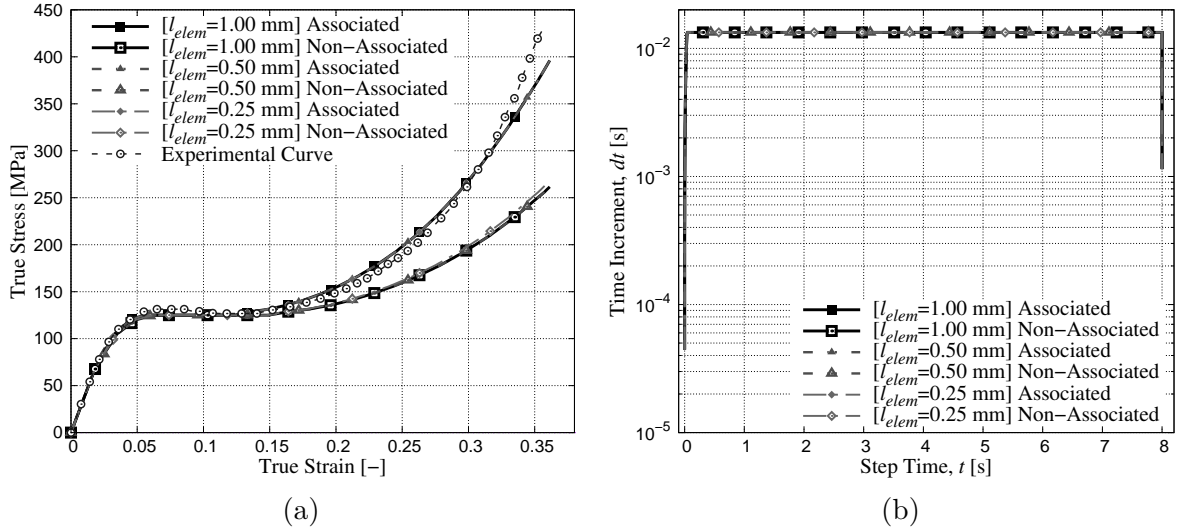


**Figure 5:** Simulation results for cylinder compression test. (a): Homogenised stress-strain relationship. (b): Time incrementation status.

Figure 5(a) show the homogenised volume-averaged stress-strain curves and the experimental result are highly concurrent to the single element test in compression. With converging results for the mesh geometries of different element sizes,  $l_{elem}$ , the mesh independence of the proposed implementation of constitutive mathematical model can be clearly affirmed.

The time increment remains fairly consistent to the specified maximum time increment,  $dt = 0.0133$ s through the course of simulation in figure 5(b). A good level of mesh size ( $l_{elem}$ ) independence is obtained for strain as significant as 40%. The continuity of the incrementation process exhibited by the proposed non-iterative scheme is solid and robust.

## 5 CONCLUSIONS

The work introduces a rate-independent elastoplastic continuum model described by the paraboloidal yield criterion employing a non-iterative numerical scheme for associated

and non-associated flow rules. The consistent tangent moduli derived for both flow rules assures convergent results. Knowledge of an exact, efficient and unambiguous computation of plastic strain increment is the novelty of this research.

The numerical implementations yielded sound results relative to the experimental validations under various loading conditions for generic epoxy polymer under large strains. A method to extrapolate yield stress evolution with plastic strain at hyper-elastoplastic regime was assumed and tested. The compression results for associated flow rule showed complete conformance, while the non-associated plasticity diverged under hyper-elastoplastic conditions.

The tests performed demonstrate efficiency and robustness of the non-iterative algorithmic approach. Single element test under tension, compression and shear has been tested and validated. Similarly, a compression test on a cylinder-shaped specimen has been performed undergoing very large deformations with the aim of assessing mesh convergence and numerical stability.

The current research work is further expanded by coupling rate-dependent and thermal parameters of the polymer constitutive model.

## ACKNOWLEDGEMENTS

**V. Laheri:** Financial support from “Bijzonder Onderzoeksfonds” (BOF.STG.2018.0030.01) by Ghent University is gratefully acknowledged.

**P. Hao:** Funded by the ICON project “ProPeL”, which fits in the MacroModelMat (M3) research program, coordinated by Siemens (Siemens Digital Industries Software, Belgium), and funded by SIM (Strategic Initiative Materials in Flanders) and VLAIO (Flemish government agency Flanders Innovation & Entrepreneurship).

## REFERENCES

- [1] N. W. Tschoegl. Failure surfaces in principal stress space. *Polymer Science Symposium*, 32:239–267, 1971.
- [2] A. R. Melro. Analytical and numerical modelling of damage and fracture of advanced composites. , 2011-02.
- [3] B. D. Coleman and W. Noll. The thermodynamics of elastic materials with heat conduction and viscosity. *The Foundations of Mechanics and Thermodynamics*, page 2, 1963.
- [4] S. Kolling, A. Haufe, and M. Feucht. SAMP: A semi-analytical model for the simulation of polymers. In *DYNAmore GmbH*, pages 27–52, 2005.
- [5] B. C. Duncan, G. D. Dean, and B. E. Read. Prediction of the performance of adhesives under impact loading. *Project PAJ2 Dynamic Performance of Adhesively Bonded Joints*, CMMT(B)162:7, 1998-01.

- [6] A.R. Melro, P.P. Camanho, F.M. Andrade Pires, and S.T. Pinho. Numerical simulation of the non-linear deformation of 5-harness satin weaves. *Computational Materials Science*, 61:116–126, 2012-08.
- [7] A.R. Melro, P.P. Camanho, F.M. Andrade Pires, and S.T. Pinho. Micromechanical analysis of polymer composites reinforced by unidirectional fibres: Part i – constitutive modelling. *International Journal of Solids and Structures*, 50(11):1897–1905, 2013-06.
- [8] A.R. Melro, P.P. Camanho, F.M. Andrade Pires, and S.T. Pinho. Micromechanical analysis of polymer composites reinforced by unidirectional fibres: Part II – micromechanical analyses. *International Journal of Solids and Structures*, 50(11):1906–1915, 2013-06.
- [9] A. Arteiro, G. Catalanotti, A.R. Melro, P. Linde, and P.P. Camanho. Micro-mechanical analysis of the in situ effect in polymer composite laminates. *Composite Structures*, 116:827–840, 2014-09.
- [10] A. Arteiro, G. Catalanotti, A.R. Melro, P. Linde, and P.P. Camanho. Micro-mechanical analysis of the effect of ply thickness on the transverse compressive strength of polymer composites. *Composites Part A: Applied Science and Manufacturing*, 79:127–137, 2015-12.
- [11] R. P. Tavares, A. R. Melro, M. A. Bessa, A. Turon, W. K. Liu, and P. P. Camanho. Mechanics of hybrid polymer composites: analytical and computational study. *Computational Mechanics*, 57(3):405–421, 2016-03.
- [12] L.F. Varandas, A. Arteiro, M.A. Bessa, A.R. Melro, and G. Catalanotti. The effect of through-thickness compressive stress on mode II interlaminar crack propagation: A computational micromechanics approach. *Composite Structures*, 182:326–334, 2017-12.
- [13] H. Ghayoor, C. C. Marsden, S. V. Hoa, and A. R. Melro. Numerical analysis of resin-rich areas and their effects on failure initiation of composites. *Composites Part A: Applied Science and Manufacturing*, 117:125–133, 2019-02.
- [14] L. F. Varandas, G. Catalanotti, A. R. Melro, and B. G. Falzon. On the importance of nesting considerations for accurate computational damage modelling in 2d woven composite materials. *Computational Materials Science*, 172:109323, 2020-02.
- [15] L.F. Varandas, G. Catalanotti, A.R. Melro, R.P. Tavares, and B.G. Falzon. Micromechanical modelling of the longitudinal compressive and tensile failure of unidirectional composites: The effect of fibre misalignment introduced via a stochastic process. *International Journal of Solids and Structures*, 203:157–176, 2020-10.

- [16] F.J. Guild, K.D. Potter, J. Heinrich, R.D. Adams, and M.R. Winsom. Understanding and control of adhesive crack propagation in bonded joints between carbon fibre composite adherends II. finite element analysis. *International Journal of Adhesion and Adhesives*, 21(6):445–453, 2001-01.
- [17] B. Fiedler, M. Hojo, S. Ochiai, K. Schulte, and M. Ando. Failure behavior of an epoxy matrix under different kinds of static loading. *Composites Science and Technology*, 61(11):1615–1624, 2001-08.